

Optimization of non-ideal multimode interference devices

Brian R. West *, David V. Plant

Department of Electrical and Computer Engineering, Photonic Systems Group, McGill University, Montreal, QC, Canada H3A 2A7

Received 7 February 2007; received in revised form 9 May 2007; accepted 30 June 2007

Abstract

Multimode interference devices are examined outside of the step-index, paraxial regime. To determine the optimum length of these devices, we maximize the projection of the propagated field in the multimode section onto the desired field profile. By consideration of the orthogonality among the guided modes, this reduces to a criterion of minimum weighted phase errors at the imaging plane, with no dependence on the actual mode field profiles. The results are confirmed by comparison with mode propagation analysis simulations. This analysis is immediately applicable to the design of multimode interference devices in weakly-guiding geometries such as shallow ridge waveguides, weakly-guiding materials systems such as photosensitive glasses and polymers, and waveguides with graded claddings and/or weak index gradients in the core, such as those formed through diffusive processes. The procedure is also used to explain the presence of the recently observed pseudo-self-image, which is not predicted by the standard theory of multimode interference.

© 2007 Elsevier B.V. All rights reserved.

1. Introduction

Periodic self-imaging in planar multimode waveguides, first suggested by Bryngdahl [1] and elaborated upon by Ulrich [2], has gained widespread interest in the photonics community. Essentially a guided-wave implementation of the Talbot effect [3,4], self-imaging has been used to design $1 \times N$ splitters [5], multiplexers [6], dual-band splitters [7], switches [8], etc. The compact size, loose fabrication tolerance, and wide optical bandwidth [9] of such multimode interference (MMI) devices are often cited as decisive factors in the adoption of these structures over those exploiting alternate physical principles such as directional coupling or adiabatic modal evolution.

The fundamental characteristic of step-index waveguides that permits their use in self-imaging is a distribution of propagation constants that is – within the paraxial approximation – quadratic. As will be reviewed in the following section, propagation of an input image through a bound

medium with a quadratic mode spectrum results in the formation of discrete imaging planes in which the modes have a well-defined phase relation, leading to direct, mirrored, and multiple self-images. In reality, the spectrum of propagation constants in a step-index multimode waveguide is not precisely quadratic, and thus the formation of self-images is not exact. This was discussed by Ulrich [2] and Ulrich and Kamiya [10], who pointed out that the optimum imaging length differs from the paraxial imaging length in the case of strong guiding. A more common source of non-idealities in self-imaging arises from the use of weak guiding. Many photonic materials such as polymers and glasses have a very small index difference between core and cladding, which provides many desirable characteristics such as low thermal and polarization dependence. However, the resulting weak guidance produces a waveguide with a highly non-parabolic mode spectrum. In addition, diffusive waveguide fabrication processes result in the formation of gradient-index waveguides, which also have a non-parabolic mode spectrum. Despite this fact, MMI devices have been successfully fabricated by deep-ultraviolet modification of polymers [11], and by ion exchange in glass [12,13]. These devices are generally designed by trial

* Corresponding author. Tel.: +1 514 398 2531; fax: +1 514 398 5208.
E-mail addresses: Brian.West@mail.mcgill.ca (B.R. West), david.plant@mcgill.ca (D.V. Plant).

and error, or by using purely numerical optimization procedures that generally involve the calculation of overlap integrals between the fields in the multimode and access waveguides [14].

In this work, we abandon the assumption that the propagation constants of the multimode waveguide have a quadratic distribution. Given the actual propagation constants (calculated using any available type of mode solver), the optimum length of the multimode waveguide is determined by maximizing the correlation between the actual and desired field distributions, a procedure that requires knowledge of only the propagation constants and modal expansion coefficients and not the modal field profiles themselves. In the following section, we review the relevant theory of paraxial self-imaging. A description of the optimization criterion is given in Section 3. In Section 4, three examples are provided; self-imaging in a “perfectly-guided” structure in which non-paraxial effects are non-negligible, a weakly-guided step-index MMI device and one with an index gradient in the cladding. Finally, in Section 5, we use this theory to explain the phenomenon of “pseudo-self-imaging,” in which self-imaging appears at planes that are not predicted by the paraxial theory.

2. Multimode imaging in step-index waveguides

We present here a brief review of multimode self-imaging in a step-index waveguide (Fig. 1), as described in Ref. [15]. The results of this analysis will describe the paraxial image with respect to which the actual image will be compared. We assume that the waveguide is two-dimensional, $n = n(x, z)$; three-dimensional waveguides can be reduced to two dimensions by application of the effective index method, with no loss of generality provided that the waveguide supports a single vertical mode.

At a free-space wavelength λ_0 , the waveguide supports m guided modes, with modal index $v = 0, 1, \dots, (m - 1)$. The modes have sinusoidal profiles within the core, with propagation constants β_v and lateral wavenumbers k_{xv} , related by the dispersion equation

$$\beta_v^2 = (k_0 n_{co})^2 - k_{xv}^2, \quad (1)$$

where n_{co} is the core index, $k_0 = 2\pi/\lambda_0$ is the free-space wavenumber, and

$$k_{xv} = \frac{(v + 1)\pi}{W_e}. \quad (2)$$

In (2), W_e is the effective width of the waveguide, which accounts for the finite penetration depth of the mode into the cladding. Although this penetration depth is dependent on mode number, the difference among modes is negligible in the case of strong guiding, so all effective widths are assumed identical and equal to

$$W_e \cong W + \left(\frac{\lambda_0}{\pi}\right) \left(\frac{n_{cl}}{n_{co}}\right)^{2\sigma} (n_{co}^2 - n_{cl}^2)^{-1/2}, \quad (3)$$

where $\sigma = 0$ for TE polarization and 1 for TM, W is the physical width of the waveguide, and n_{cl} is the cladding index. A few of the lowest-order modes in this waveguide are illustrated in Fig. 1.

Invoking the paraxial approximation by expanding (1) to second order in $(v + 1)$ yields

$$\beta_v \cong k_0 n_{co} - \frac{(v + 1)^2 \pi \lambda_0}{4 n_{co} W_e^2}. \quad (4)$$

The spacing of the propagation constants can thus be expressed as

$$(\beta_0 - \beta_v) \cong \frac{v(v + 2)\pi}{3L_\pi}, \quad (5)$$

where

$$L_\pi = \frac{\pi}{\beta_0 - \beta_1} = \frac{4 n_{co} W_e^2}{3 \lambda_0} \quad (6)$$

is the beat length of the two lowest-order modes. The parabolic distribution of propagation constants shown in (5) is the crucial element in self-imaging. In the following section, we will examine the consequences of the presence of higher-order terms in the expansion of (1).

Propagation of an input field through the multimode waveguide is modeled using mode propagation analysis (MPA). The input field $\Psi(x, z = 0)$ can be expressed as an expansion in the waveguide eigenmodes $\psi_v(x)$,

$$\Psi(x, 0) = \sum_{v=0}^{m-1} c_v \psi_v(x), \quad (7)$$

with the time dependence $\exp(i\omega t)$ suppressed, and with expansion coefficients

$$c_v = \frac{\int_{-\infty}^{\infty} \Psi(x, 0) \psi_v(x) dx}{\left(\int_{-\infty}^{\infty} \psi_v^2(x) dx\right)^{1/2}}. \quad (8)$$

Strictly speaking, the sum in (7) should include radiation modes as well, but for all practical applications, the spatial spectrum of $\Psi(x, 0)$ is sufficiently limited that excitation of radiation modes has negligible impact at the image plane. After propagating a distance z , the field takes the form

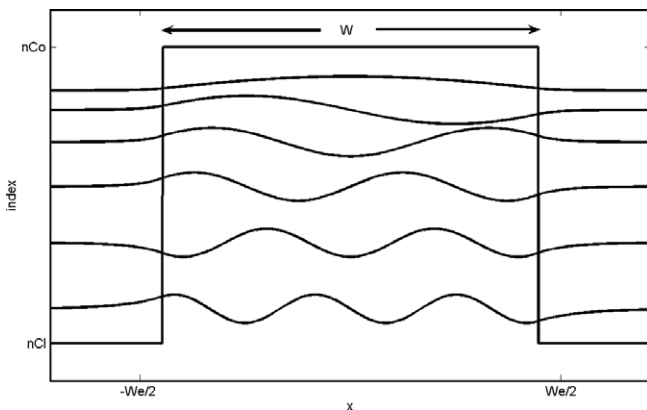


Fig. 1. Transverse field profiles of the first six guided modes in a multimode slab waveguide, illustrating the concept of effective width W_e .

$$\Psi(x, z) = \sum_{v=0}^{m-1} c_v \psi_v(x) \exp[i(\beta_0 - \beta_v)z], \quad (9)$$

where a non-significant overall phase factor $\exp(-i\beta_0 z)$ has been removed from the sum. Finally, substituting (5) into (9) leads to the following form for the field at plane z :

$$\Psi(x, z) = \sum_{v=0}^{m-1} c_v \psi_v(x) \exp\left[i \frac{v(v+2)\pi}{3L_\pi} z\right]. \quad (10)$$

Comparing (7) and (10), it is apparent that $\Psi(x, z)$ will be an image of $\Psi(x, 0)$ if

$$\exp\left[i \frac{v(v+2)\pi}{3L_\pi} z\right] = 1 \quad \text{or} \quad (-1)^v. \quad (11)$$

This condition is met at the planes

$$z = p(3L_\pi), \quad p = 0, 1, 2, \dots \quad (12)$$

With p even, (10) represents a direct image, $\Psi(x, z) = \Psi(x, 0)$. When p is odd, using the properties

$$v(v+2) = \begin{cases} \text{even} & \text{for } v \text{ even,} \\ \text{odd} & \text{for } v \text{ odd,} \end{cases} \quad (13)$$

and

$$\psi_v(-x) = \begin{cases} \psi_v(x) & \text{for } v \text{ even,} \\ -\psi_v(x) & \text{for } v \text{ odd,} \end{cases} \quad (14)$$

we see that the image will be mirrored about the plane $x = 0$; $\Psi(x, z) = \Psi(-x, 0)$. Utilizing the direct and mirrored self-images leads to bar- and cross-couplers, respectively. Often, the input field will be symmetric about the x -plane, in which case only even modes will be excited. In this case, images of the input will be found at planes [16]

$$z = p(3L_\pi/4), \quad p = 0, 1, 2, \dots \quad (15)$$

It is also possible to obtain N -fold multiple self-images at the planes [17]

$$z = p(3L_\pi/N), \quad p = 0, 1, 2, \dots \quad (16)$$

or, in the symmetric input case,

$$z = p(3L_\pi/4N), \quad p = 0, 1, 2, \dots \quad (17)$$

provided that a minimum of N modes in the multimode guide are excited by the input image, in order to provide adequate spatial resolution for N -fold imaging. For most practical devices, the first non-trivial image plane ($p = 1$) is used in order to minimize the device length. In the following section, we shall see that in realistic MMI devices, the optimal imaging planes are offset with respect to those calculated via (12), (15)–(17).

3. Multimode imaging beyond the paraxial approximation

In real waveguides, the distribution of propagation constants is not precisely quadratic as assumed in (4), and thus the relation (10) is inaccurate. As an example, expanding (1) to fourth order in $(v+1)$ results in

$$\beta_v \cong k_0 n_{co} - \frac{(v+1)^2 \pi \lambda_0}{4n_{co} W_e^2} - \frac{(v+1)^4 \pi \lambda_0^3}{64n_{co}^3 W_e^4}, \quad (18)$$

and thus the total field at a distance z from the input plane is

$$\Psi(x, z) = \sum_{v=0}^{m-1} c_v \psi_v(x) \exp[i\varphi_v(z)] \quad (19)$$

with the modal phases derived analogously to those in (5),

$$\varphi_v(z) = \left\{ \frac{v(v+2)}{3L_\pi} + \frac{[(v+1)^4 - 1]}{3L_\pi} \left[\frac{\lambda_0}{n_{co} W_e} \right]^2 \right\} \pi z. \quad (20)$$

For all MMI devices, the term $(\lambda_0/n_{co} W_e)^2 \ll 1$, so no realistic imaging length z exists such that $\psi_v(z)$ satisfies any appropriate self-imaging relationship (such as (11)) for all v . It should be noted that perfect self-images at very large multiples of L_π may exist, however these are not practical in the design of compact devices with finite propagation loss, and will not be discussed further. In this case, it is inevitable that phase errors will occur, with magnitudes increasing proportionally to $(v+1)^4 - 1$.

In a manner similar to the balancing of aberrations in a geometrical optical system by a longitudinal shift of the image plane, we wish to develop a procedure by which the imaging quality can be optimized by altering the length of the multimode waveguide. Geometrical aberration theory has been used with some success in the study of free-space Talbot imaging with high magnification [18], but loses validity in most cases of interest in MMI design as it does not take into account the coherent superposition of the guided modes. Ulrich and Kamiya [10] proposed an analytical solution to find the best image plane in a non-paraxial MMI device, but their method requires a very large number of guided modes to be present, with negligible excitation of the modes near cutoff, and it is not valid for weakly-guided or gradient-index waveguides.

We choose to optimize the device length by maximizing the projection of the field obtained at an arbitrary image plane z onto the desired output field profile. Denoting the desired quantities by a tilde (\sim) and using (19) to express the field at a plane z , a figure of merit $F(z)$ is created:

$$\begin{aligned} F(z) &= \left| \langle \tilde{\Psi}(x, z) | \Psi(x, z) \rangle_x \right|^2 \\ &= \left| \int_x \sum_v c_v^* \psi_v^*(x) \exp[-i\tilde{\varphi}_v(z)] \sum_\mu c_\mu \psi_\mu(x) \exp[i\varphi_\mu(z)] dx \right|^2 \\ &= \left| \sum_v |c_v|^2 \exp\{i[\varphi_v(z) - \tilde{\varphi}_v(z)]\} \right|^2. \end{aligned} \quad (21)$$

Taking the absolute value squared of the inner product ensures that $F(z)$ is a real quantity, with $0 \leq F(z) \leq \sum |c_v|^2$ (≈ 1 for negligible excitation of radiation modes). It is proportional to the power coupling between the multimode guide and the desired output image, which is generally

the quantity of interest. This figure of merit is particularly appealing in that its calculation does not require any integration, as the mode field profiles vanish from (21) due to orthogonality.

Two important characteristics of $F(z)$ are readily apparent and warrant further discussion. First, each term in the sum is proportional to the square of that mode’s excitation coefficient, and thus the optimal design of the multimode waveguide depends not only on the index profile of the multimode guide, but also on the input field, through (8). This shows that the spatial resolution of the device cannot be increased indefinitely by using a narrow (high-spatial-bandwidth) input guide, as the phase errors in higher-order modes will become more prominent; this limitation was described in [10]. Limiting the spatial bandwidth to reduce phase errors is similar in concept to the reduction of aberrations in a geometrical optical system either by apodizing or by reducing the size of the limiting aperture. The second important characteristic is that each term in $F(z)$ is periodic in phase error. A mode that is dephased by an integer multiple of 2π will not have any detrimental effect on the self-imaging; this has no analog in the geometrical case.

4. Examples

4.1. Step-index slab waveguide without paraxial approximation

As a first example, we investigate a “perfectly-guided” step-index waveguide, such as that formed by an air gap between two perfect mirrors [19]. The assumption of perfect guiding is used only to force the condition that $W_c = W$ is identical for all modes. The waveguide has a width of $W = 20 \mu\text{m}$, with $n_{co} = 1$ and $\lambda_0 = 1.55 \mu\text{m}$. The input image is Gaussian and symmetric with $4 \mu\text{m}$ full-width ($1/e^2$ power), and we wish to achieve 1×2 splitting. As the input image is symmetric with respect to the multimode waveguide, odd modes are not excited. From (6) and (17) with $p = 1$ and $N = 2$, we find that the paraxial imaging length is $129.0 \mu\text{m}$. Table 1 lists the propagation constants and expansion coefficients of the first 6 even modes (higher-order modes have negligible excitation), calculated using both the fourth-order approximation (18) and the fully accurate representation (1). Fig. 2a shows $F(z)$ in the vicinity of the paraxial imaging length, calculated using

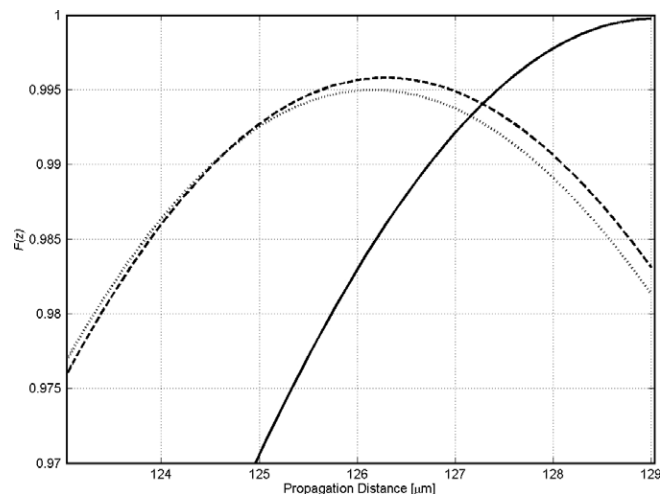


Fig. 2a. $F(z)$ for 1×2 splitting in a perfectly guided slab waveguide. Solid line: paraxial approximation (paraxial image length = $129.0 \mu\text{m}$). Dashed line: fourth-order approximation (optimum image length = $126.3 \mu\text{m}$). Dotted line: fully accurate propagation constants (optimum image length = $126.1 \mu\text{m}$).

the desired phases $\tilde{\varphi}_v = v(v + 2)\pi/8$ (see (17)). From this figure, we see that the optimum imaging length is $126.3 \mu\text{m}$ (to fourth order) or $126.1 \mu\text{m}$ (fully accurate). The power cross-section at the paraxial and optimized image planes, calculated using MPA, is shown in Fig. 2b. Although the optimized image plane is shifted by only $2.9 \mu\text{m}$ from the paraxial image plane, there is a noticeable improvement in the self-image quality.

4.2. Weakly-guided slab waveguide

Next, we examine the design of a 1×4 splitter in a weakly-guided system with cladding index $n_{cl} = 1.500$ and $n_{co} = 1.505$. A multimode guide of $80 \mu\text{m}$ width is used, with a symmetric Gaussian input of $8 \mu\text{m}$ full width. At a wavelength of $1.55 \mu\text{m}$, using (3), (6), and (17), the paraxial 1×4 imaging length is found to equal $1713.8 \mu\text{m}$. Applying a one-dimensional finite difference method to solve for the propagation constants, and using the desired modal phases of $\tilde{\varphi}_v = v(v + 2)\pi/16$, we see that $F(z)$ is maximized at $1754.5 \mu\text{m}$. Power cross-sections calculated by MPA are shown in Fig. 3, and it is readily apparent that the uniformity of the 4-fold images is greatly improved in the optimized image plane.

4.3. Gradient-index waveguide

To fully explore the versatility of our design optimization method, we now examine an MMI structure that is formed in a gradient-index waveguide. In diffusive waveguide fabrication processes such as ion exchange, the waveguide can be considered as having a core of constant index, with a cladding that is graded due to side-diffusion under the mask [20] (note that only the transverse index distribution is relevant here; the waveguide is assumed to support a

Table 1
Propagation constants and expansion coefficients for the 1×2 splitter described in Section 4.1

Mode number, v	β_v (μm^{-1}) [from (18)]	β_v (μm^{-1}) [from (1)]	c_v
0	4.050623	4.050623	0.690787
2	4.026185	4.026184	0.567054
4	3.976868	3.976855	0.382090
6	3.901797	3.901692	0.211342
8	3.799655	3.799162	0.095958
10	3.668687	3.666970	0.035764

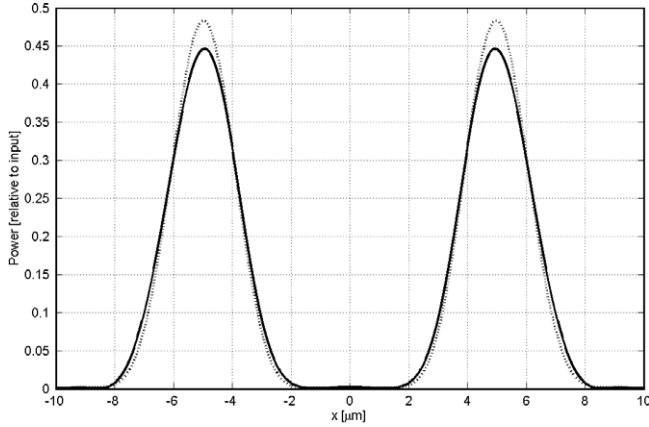


Fig. 2b. Power cross-sections in a perfectly guiding multimode waveguide. Solid line: paraxial image plane (129.0 μm). Dotted line: optimized image plane (126.1 μm).

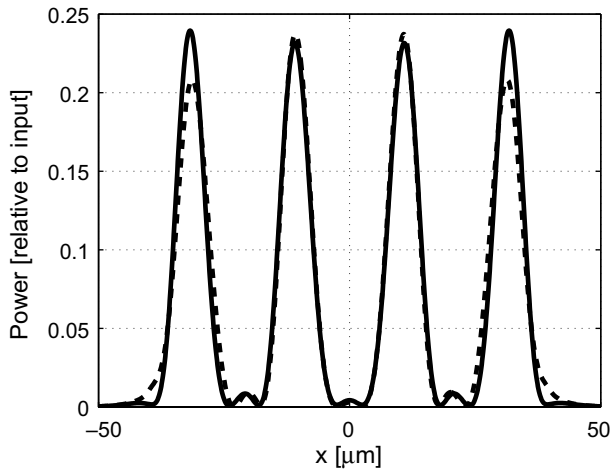


Fig. 3. Power cross-sections in a weakly-guiding multimode waveguide (parameters are given in the text). Solid line: optimized image plane (1754.5 μm). Dashed line: paraxial image plane (1713.8 μm).

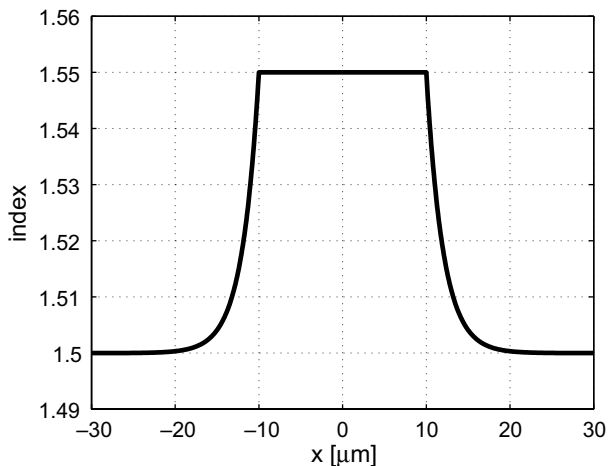


Fig. 4. Refractive index profile of the waveguide analyzed in Section 4.3.

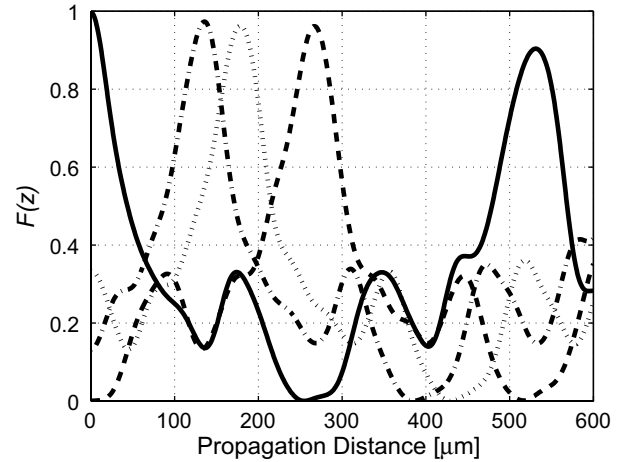


Fig. 5. $F(z)$ for $1 \times N$ splitting in the waveguide described in Section 4.3. Solid line: $N = 1$ (optimum image length = 531.2 μm). Dashed line: $N = 2$ (optimum image length = 266.9 μm). Dotted line: $N = 3$ (optimum image length = 178.4 μm). Dash-dotted line: $N = 4$ (optimum image length = 135.5 μm).

single vertical mode, and the entire structure can be reduced to two dimensions through application of the effective index method as mentioned in Section 2). We will now use (21) to design a $1 \times N$ splitter in a multimode waveguide with index profile

$$n(x) = \begin{cases} n_{\text{cl}} + \Delta n, & |x| \leq W/2, \\ n_{\text{cl}} + \Delta n \exp[-\alpha(|x| - \frac{W}{2})], & |x| \geq W/2, \end{cases} \quad (22)$$

with $n_{\text{cl}} = 1.50$, $\Delta n = 0.05$, $\alpha = 0.5 \mu\text{m}^{-1}$, and $W = 20 \mu\text{m}$. The index profile is shown in Fig. 4. At $\lambda_0 = 1.55 \mu\text{m}$, with a Gaussian input with 4 μm full-width, curves of $F(z)$ for $N = 1-4$ are calculated using $\tilde{\varphi}_v = v(v+2)\pi/4N$, and are plotted in Fig. 5. The power cross-sections at the optimized imaging lengths are provided in Fig. 6. It is apparent that the total insertion loss decreases with N , due to the shorter propagation length over which the modes are able to de-phase.

5. Pseudo-self-imaging

The pseudo-self-image (PSI), identified recently by Hong and Lee [21], and Hong et al. [22] occurs when a self-image of acceptable quality is formed in an image plane that is not predicted by the theory presented in Section 2. We show here that the existence of these PSIs is predicted by our optimization method. The structure described in Ref. [21] is designed in buried silica, with an index difference of 0.75%, a width of 18 μm and a thickness of 6 μm . Access waveguides have a square cross-section of 6 μm width, and are offset from the multimode waveguide axis by 6 μm . Standard MMI theory predicts a series of alternating mirrored and direct self-images, with a distance of $6L_\pi$ between direct self-images, as shown in Eq. (12). However, the authors of [21,22] demonstrated via simulation and experiment that each direct (mirrored) self-image

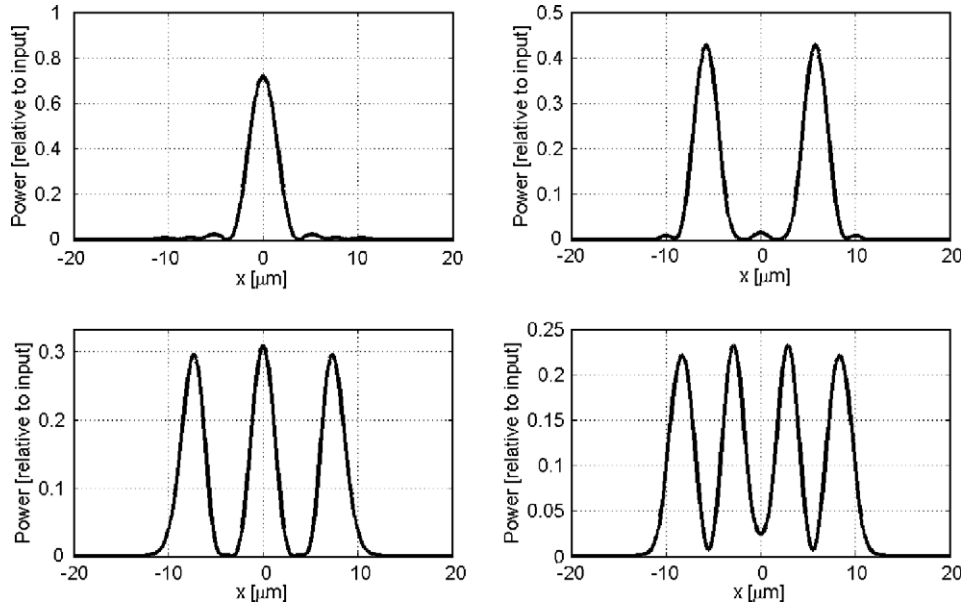


Fig. 6. Power cross-sections at the optimized $1 \times N$ image planes for the waveguide described in Section 4.3: (a) $N = 1$, $L_1 = 531.2 \mu\text{m}$; (b) $N = 2$, $L_2 = 266.9 \mu\text{m}$; (c) $N = 3$, $L_3 = 178.4 \mu\text{m}$; (d) $N = 4$, $L_4 = 135.5 \mu\text{m}$.

Table 2
Propagation constants and expansion coefficients for the pseudo-self-imaging device described in Section 5

Mode number, ν	$\beta_\nu (\mu\text{m}^{-1})$	c_ν
0	5.888899	-0.553698
1	5.883226	-0.689314
2	5.874017	0.443861
3	5.862215	0.139311

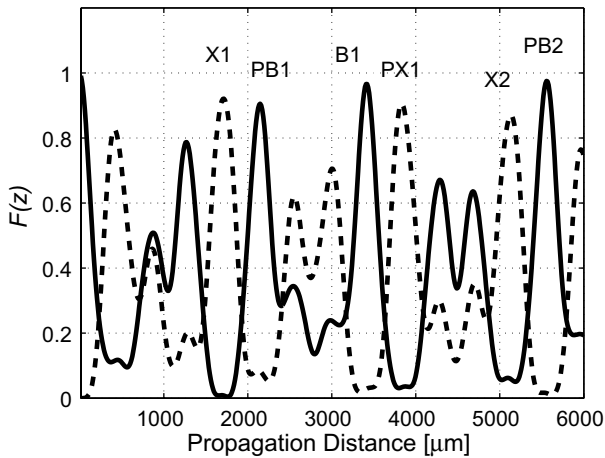


Fig. 7. $F(z)$ for the waveguide described in Section 5. Solid line: bar state. Dashed line: cross state. Peak labels: X1, first cross state; PB1, first pseudo-bar state; B1, first bar state; PX1, first pseudo-cross state; X2, second cross-state; PB2, second pseudo-bar state.

is followed closely by a mirrored (direct) one, a phenomenon that shows promise in the design of compact coarse wavelength division multiplexers [23]. Using a two-dimensional semivectorial finite difference mode solver [24] for

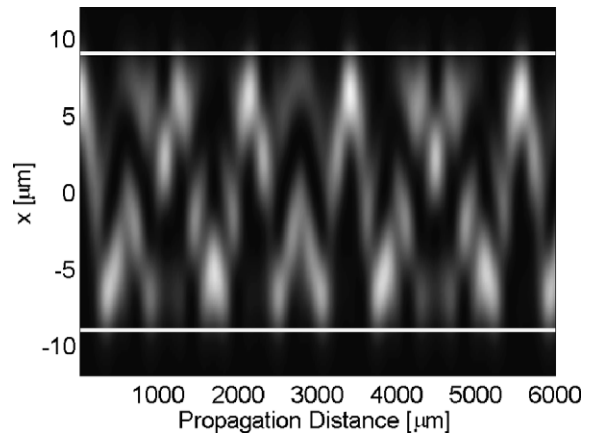


Fig. 8. Power profile within the waveguide described in Section 5.

quasi-TE polarization, the multimode waveguide is shown to support four guided modes, with propagation constants and excitation coefficients given in Table 2. The figure of merit $F(z)$ is shown in Fig. 7 for both direct and mirrored self-imaging, with both self-images and pseudo-self-images indicated. The power profile within the multimode guide is shown in Fig. 8. In addition to the self-images located at 1710.7, 3413.5, and 5132.0 μm , pseudo-self-images of very high quality appear at 2146.0, 3831.0, and 5559.6 μm . The slight discrepancy between these imaging lengths and those found in [21] is due only to an ambiguity in absolute refractive index and polarization in that reference.

6. Conclusions

We have developed a simple figure of merit to optimize the length of non-ideal multimode interference devices.

Based on a maximization of the projection of the field at an arbitrary image plane onto the desired output field, the figure of merit reduces to a minimization of the sum of phase errors of each mode, weighted by the proportion of power contained in that mode. Application of this optimization method is simple and rapid as it does not require calculation of overlap integrals at each potential imaging plane. The method is illustrated by the analysis of perfectly-guided (non-paraxial), weakly-guided, and gradient-index waveguides.

Acknowledgement

This work was supported by the Natural Sciences and Engineering Research Council (NSERC) and industrial and government partners, through the Agile All-Photonic Networks (AAPN) Research Network.

References

- [1] O. Bryngdahl, *J. Opt. Soc. Am.* 63 (1973) 416.
- [2] R. Ulrich, *Opt. Commun.* 13 (1975) 259.
- [3] H.F. Talbot, *London Edinburgh Philos. Mag.* 9 (1836) 401.
- [4] L. Rayleigh, *London Edinburgh Philos. Mag.* 11 (1881) 195.
- [5] T. Rasmussen, J.K. Rasmussen, J.H. Povlsen, *J. Lightwave Technol.* 13 (1995) 2069.
- [6] A. Bakhtazad, J.N. McMullin, C.J. Haugen, R.G. DeCorby, *Opt. Express* 9 (2001) 178.
- [7] L.-W. Chung, S.-L. Lee, Y.-J. Lin, *Opt. Express* 14 (2006) 8753.
- [8] R.M. Jenkins, J.M. Heaton, D.R. Wight, J.T. Parker, J.C.H. Birbeck, G.W. Smith, K.P. Hilton, *Appl. Phys. Lett.* 64 (1994) 684.
- [9] P.A. Besse, M. Bachmann, H. Melchior, L.B. Soldano, M.K. Smit, *J. Lightwave Technol.* 12 (1994) 1004.
- [10] R. Ulrich, T. Kamiya, *J. Opt. Soc. Am.* 68 (1978) 583.
- [11] D.G. Rabus, P. Henzi, J. Mohr, *IEEE Photon. Tech. Lett.* 17 (2005) 591.
- [12] M. Blahut, D. Kasprzak, *Opt. Appl.* 33 (2003) 613.
- [13] S. Das, D. Geraghty, S. Honkanen, N. Peyghambarian, *Proc. SPIE* 3936 (2000) 239.
- [14] B. West, S. Honkanen, *Opt. Express* 12 (2004) 2716.
- [15] L.B. Soldano, E.C.M. Pennings, *J. Lightwave Technol.* 13 (1995) 615.
- [16] E.C.M. Pennings, R.J. Deri, A. Scherer, R. Bhat, T.R. Hayes, N.C. Andreadakis, M.K. Smit, R.J. Hawkins, *Appl. Phys. Lett.* 59 (1991) 1926.
- [17] M. Bachmann, P.A. Besse, H. Melchior, *Appl. Opt.* 33 (1994) 3905.
- [18] Y. Cohen-Sabban, D. Joyeux, *J. Opt. Soc. Am.* 73 (1983) 707.
- [19] Yu.B. Ovchinnikov, *Opt. Commun.* 182 (2000) 35.
- [20] J. Albert, Ion exchange from salt melts, in: S.I. Najafi (Ed.), *Introduction to Glass Integrated Optics*, Artech House, Norwood, MA, 1992.
- [21] J.-K. Hong, S.-S. Lee, *Microwave Opt. Tech. Lett.* 48 (2006) 2354.
- [22] J.-K. Hong, S.-S. Lee, S.-D. Lee, *Opt. Lett.* 32 (2007) 1311.
- [23] J.-K. Hong, S.-S. Lee, *J. Lightwave Technol.* 25 (2007) 1264.
- [24] M.S. Stern, *IEE Proc. J.* 135 (1988) 56.